Ionics (2015) 21:111–124
DOI 10.1007/s11581-014-1157-5

ORIGINAL PAPER

Electrical and transport properties of NH_4Br-doped cornstarch-based solid biopolymer electrolyte

M. F. Shukur · M. F. Z. Kadir

Received: 18 February 2014 / Revised: 6 May 2014 / Accepted: 18 May 2014 / Published online: 31 May 2014

Abstract In this work, cornstarch-based electrolytes are doped with ammonium bromide (NH_4Br) and plasticized with glycerol. Starch-NH_4Br complexation is evidenced from the Fourier transform infrared (FTIR) spectroscopy results. A room temperature conductivity of $(5.57\pm1.88)\times10^{-5}$ S cm^{-1} obtained by 70 wt% starch–30 wt% NH_4Br electrolyte is enhanced to $(1.80\pm0.26)\times10^{-3}$ S cm^{-1} with the addition of 30 wt% glycerol. All electrolytes exhibit Arrhenius behavior. The conduction mechanism of 70 wt% starch–30 wt% NH_4Br electrolyte and 49 wt% starch–21 wt% NH_4Br–30 wt% glycerol electrolyte follows overlapping large polaron tunneling (OLPT) and correlated barrier hopping (CBH) models, respectively. The transference number of ion (t_{ion}) and proton (t_p) is found to be 0.98 and 0.35, respectively, for 49 wt% starch–21 wt% NH_4Br–30 wt% glycerol electrolyte. The decomposition voltage of 49 wt% starch–21 wt% NH_4Br–30 wt% glycerol electrolyte is 1.66 V.

Keywords Solid polymer electrolyte · Starch · Ammonium bromide · Glycerol · Conductivity · Transference number

Introduction

Ionic conductors are regarded as key components in electrochemical devices since the ionic conduction has a strong influence on the devices performance [1, 2]. Liquid electrolytes as ionic conductors are preferable because of their high ionic conductivity [3, 4]. However, the use of liquid electrolyte in electrochemical devices suffers a lot of problems such as leakage, corrosion, and solvent evaporation at high temperature [5, 6]. Hence, researchers have turned their attention on solid polymer electrolytes (SPEs) which offer advantages, e.g., thermally stable, ability to eliminate corrosive solvent and harmful gas formation, and low volatility with easy handling [7]. Synthetic polymers have been widely used as polymer host in SPEs but most of them are insoluble in solvents [8]. Besides, most of synthetic polymers are non-biodegradable which can cause environmental problems [9].

Natural polymers have been used as polymer host in electrolyte due to their chemical structure differences, richness in nature, and they're economical and principally biodegradable [10]. In this work, cornstarch is of interest. Starch is composed of a mixture of linear polysaccharide, amylose and branched polysaccharide, and amylopectin [11]. Figure 1 shows the structure of both amylose and amylopectin [12]. Both polysaccharides composed of D-glucose units joined by α-1,4′-glucosidic linkages while amylopectin also contains α-1,6′-glucosidic linkages [12]. According to Khiar and Arof [12], the cations of salt would be more easily attached to the amylose compound rather than the amylopectin because the α-1,4′-glucosidic linkages of amylose are more stable and less steric than the α-1,6′-glucosidic linkages of amylopectin. Thus, in this work, the polymer–salt interaction is expected to occur at the functional groups in amylose, which will be discussed in the "Results and Discussion" section.

Proton-conducting SPEs have been recognized for their suitability in the application of low-energy density devices [13, 14]. Strong inorganic acids such as phosphoric acid (H_3PO_4) [15] and sulfuric acid (H_2SO_4) [16] have been used as proton donor for SPEs. However, polymer-inorganic acid complexes suffer from chemical degradation and mechanical integrity causing them unsuitable for practical applications [17]. Therefore, a lot of ammonium salts have been used to

M. F. Shukur
Institute of Graduate Studies, University of Malaya, 50603 Kuala Lumpur, Malaysia

M. F. Z. Kadir (✉)
Centre for Foundation Studies in Science, University of Malaya, 50603 Kuala Lumpur, Malaysia
e-mail: mfzkadir@um.edu.my

act as the proton donor, for example, ammonium thiocyanate (NH_4SCN) [18], ammonium nitrate (NH_4NO_3) [19], and ammonium chloride (NH_4Cl) [20]. In the present study, a proton-conducting SPE system based on starch-NH_4Br was prepared. Glycerol was added as plasticizer to enhance the conductivity of the electrolyte. The electrical characteristics of starch–NH_4Br and starch–NH_4Br–glycerol electrolytes were studied and compared.

Experimental

Preparation of SPEs

For preparation of starch–NH_4Br (salted) system, 2 g of cornstarch (Brown & Polson) were dissolved in 50 mL of 1 % acetic acid (SYSTERM) at 80 °C. The dissolved starch solutions were left to cool down to room temperature before different amounts of NH_4Br (Bendosen) were added to the solutions and stirred until homogenous solutions were obtained. For preparation of starch–NH_4Br–glycerol (plasticized) system, different amounts of glycerol (SYSTERM) were added to the highest conducting salted electrolyte solutions and stirred until homogenous solutions were obtained. All solutions were cast onto plastic Petri dishes and left to dry at room temperature. The dry samples were then kept in a desiccator filled with silica gel desiccants for further drying process.

Characterization of electrolytes

FTIR spectra were recorded using Spotlight 400 PerkinElmer spectrometer in the transmission mode of 450–4,000 cm^{-1} at a resolution of 1 cm^{-1}. Electrochemical impedance spectroscopy (EIS) measurements were performed using a HIOKI 3532–50 LCR HiTESTER from room temperature to 343 K in the frequency range of 50 Hz to 5 MHz. The electrolytes were sandwiched between two stainless steel electrodes of a conductivity holder. The value of bulk resistance (R_b) was determined from the Nyquist plots obtained. Conductivity (σ) is calculated using:

$$\sigma = \frac{t}{R_b A} \tag{1}$$

Here, t is the thickness of the electrolytes and A is the electrode–electrolyte contact area. From the impedance data, the dielectric properties of the electrolytes were analyzed. The dielectric constant (ε_r) and dielectric loss (ε_i) are defined as:

$$\varepsilon_r = \frac{Z_i}{\omega C_o \left(Z_r^2 + Z_i^2\right)} \tag{2}$$

$$\varepsilon_i = \frac{Z_r}{\omega C_o \left(Z_r^2 + Z_i^2\right)} \tag{3}$$

where C_o is the vacuum capacitance, ω is the angular frequency, Z_i is the imaginary part of impedance, and Z_r is the real part of impedance.

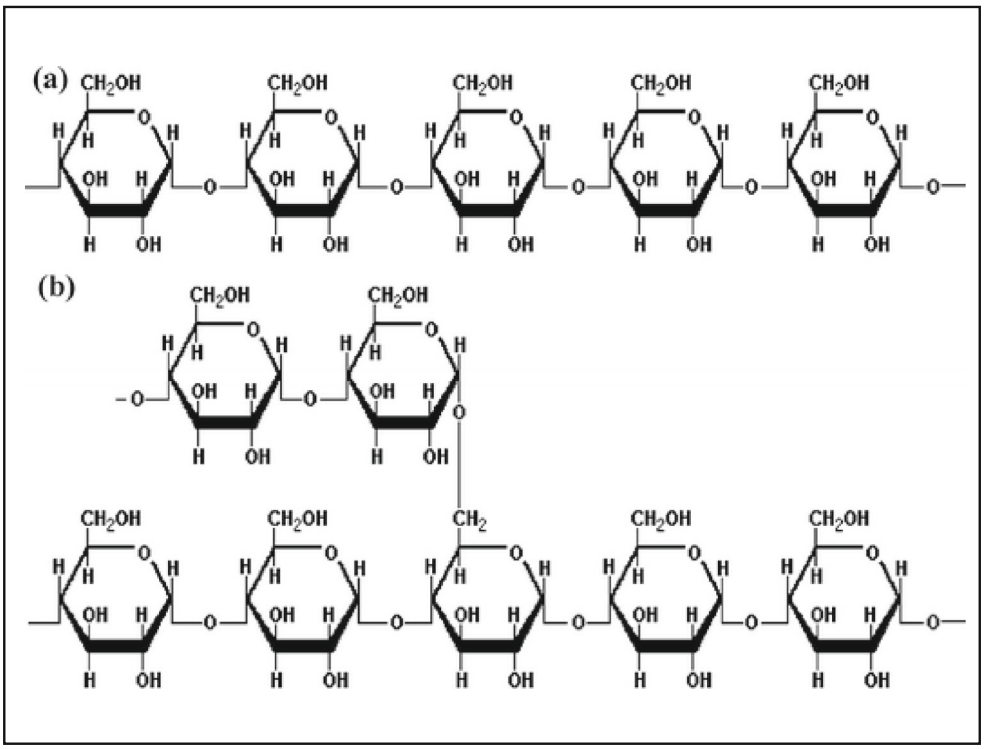

Fig. 1 Structure of **a** amylose and **b** amylopectin [12]

X-ray diffractograms were recorded using Siemens D5000 x-ray diffractometer. X-ray of 1.5406 Å wavelengths were generated by a Cu Kα source. The 2θ angle is varied from 5 to 80 ° at a resolution of 0.1 °. The degree of crystallinity (χ_c) of the electrolytes was calculated using:

$$\chi_c = \frac{A_c}{A_T} \times 100\% \quad (4)$$

where A_c and A_T are the areas of crystalline and total hump, respectively. The areas of crystalline and total hump were determined using OriginPro8 software.

The ionic transference number was measured using Wagner's DC polarization method [21]. A cell consists of the highest conducting electrolyte sandwiched by two stainless steel (SS) blocking electrodes (SS/SPE/SS) was polarized using V&A Instrument DP3003 digital DC power supply at 0.20 V. The DC current was monitored as a function of time. Measurement was done at room temperature. A combination of Wagner's DC polarization method and Watanabe's AC impedance method [22] was used to measure the proton transference number. To prepare the non-blocking electrodes, a mixture of 0.40 g manganese (IV) oxide (MnO_2) (Sigma-Aldrich), 0.04-g activated carbon (RP20, manufactured by Kuraray, Japan) and 0.08-g polytetrafluoroethylene (PTFE) was grounded and pressed using hydraulic pressing for 15 min. A cell consists of the highest conducting electrolyte sandwiched by two MnO_2 non-blocking electrodes (MnO_2/SPE/MnO_2) was polarized using V&A Instrument DP3003 digital DC power supply at 0.20 V. Impedance measurement for the MnO_2/SPE/MnO_2 cell was performed using HIOKI 3532–50 LCR HiTESTER at room temperature in the frequency range of 50 Hz to 100 kHz.

The electrochemical stability window of the highest conducting plasticized electrolyte was studied using linear sweep voltammetry (LSV). The LSV measurement was performed using Digi-IVY DY2300 potentiostat at a scan rate of 10 mV s^{-1} at room temperature. Stainless steel was used as working, counter, and reference electrodes. The potential range is from 0 to 2.5 V.

Results and discussion

FTIR analysis

According to Hema et al. [23], the cations of salt are expected to coordinate with the polar groups in the polymer matrix resulting in the polymer–salt complexation and certain infrared active modes of vibration will be affected. To investigate the complexation between polymer and salt, FTIR analysis was performed for pure starch film and starch-NH_4Br electrolytes. Figure 2a shows the FTIR spectra of selected samples in salted system in the hydroxyl band region. The hydroxyl band in the spectrum of pure starch film in Fig. 2a(i) is located at 3,280 cm^{-1}. The strong and wide absorption in the hydroxyl band region of pure starch film indicates that there are plenty of hydroxyl groups in starch [24]. The hydroxyl band of pure starch film shifts to 3,275 cm^{-1} in the presence of 10 wt% NH_4Br in Fig. 2a(ii). On addition of 25 wt% NH_4Br, the hydroxyl band has shifted to 3,260 cm^{-1} in Fig. 2a(iii) and further shifted to 3,251 cm^{-1} with the addition of 30 wt% NH_4Br in Fig. 2a(iv). It is reported that the increasing salt content in the polymer matrix has shifted the hydroxyl band of pure polymer film to lower wavenumbers [19, 25]. It has been reported that in polymer–ammonium salt complexes, the conducting charge species is H^+ ion [19, 26]. The oxygen atom of O–H carries lone pairs of electron. From the FTIR results in Fig. 2a, it can be inferred that the interaction has occurred between the H^+ ions and the oxygen atom. Appearance of new peaks can be observed with further addition of 40 wt% NH_4Br at 3,105 and 3,010 cm^{-1} in Fig. 2a(v). Those peaks are attributed to $v_{as}(NH^+)$ and $v_s(NH^+)$ modes of NH_4Br, respectively, which appear at 3,091 and 2,995 cm^{-1} in the spectrum of pure NH_4Br salt in Fig. 2a(vi). This result indicates that more salt aggregates have been formed which limit the conduction of ions. According to Stygar et al. [27], although polymer–salt interaction mainly occurs at the oxygen atom, other bands can also be affected. The FTIR spectra of selected samples in the salted system in the region of 2,890–2,970 cm^{-1} are shown in Fig. 2b. A peak which is assigned to C–H stretching mode of starch appears at 2,926 cm^{-1} in the spectrum of pure starch film in Fig. 2b(i). The increasing NH_4Br content has shifted the peak to higher wavenumbers. From Fig. 2b(iv), on addition of 30 wt% NH_4Br, the peak has shifted to 2,931 cm^{-1} and further shifted to 2,932 cm^{-1} with the addition of 35 wt% NH_4Br in Fig. 2b(v). Report by Ramesh et al. [7] shows that C–H stretching mode of starch is shifted from 2,923 to 2,931 cm^{-1} on addition of $LiPF_6$ which is comparable with our result. No peak is observed in the spectrum of 60 wt% starch–40 wt% NH_4Br electrolyte in Fig. 2b(vi) indicating the increase in crystallinity of the electrolyte. From Fig. 2c(i), a peak appears at 1,078 cm^{-1} in the spectrum of pure starch film. Ning et al. [28] observed a peak at 1,080 cm^{-1} in the spectrum of starch film which is attributed to C–O bond stretching of the C–O–C group in starch. Their result is almost similar with the present work. In Fig. 2c(ii), on addition of 25 wt% NH_4Br, the peak shifted to 1,077 cm^{-1}. Further shifting can be observed with increasing salt content. On addition of 40 wt% NH_4Br, the peak is located at 1,074 cm^{-1}. According to Ramesh et al. [7], cations interact with oxygen atoms in the C–O–C group. All these results conclude that starch has interacted with NH_4Br salt in the present work.

Figure 3a depicts the FTIR spectra for the selected samples in plasticized system in the hydroxyl band region. Due to its

multi-hydroxyl moiety structure, glycerol possesses the strong ability to interact with the polysaccharide matrix through hydrogen-bonding interactions [29]. The hydroxyl band has shifted to 3,275 cm^{-1} on addition of 10 wt% glycerol in Fig. 3a(ii). The hydroxyl band has further shifted to 3,308 cm^{-1} on addition of 30 wt% glycerol in Fig. 3a(v). This result indicates that the addition of glycerol promotes the hydrogen bonding interactions between the electrolyte components [30]. Liu et al. [31] reported that the hydroxyl band of unplasticized starch–chitosan film at 3,328.36 cm^{-1} has shifted to higher wavenumbers after the glycerol was added. According to the authors, the addition of glycerol promoted the hydrogen bonding interactions among polymers and plasticizer [31]. Figure 3b shows the FTIR spectra for the selected samples in plasticized system in the region of 955–1,055 cm^{-1}. The peak at 1,002 cm^{-1} in the spectrum of 70 wt% starch–30 wt% NH_4Br–0 wt% glycerol electrolyte in Fig. 3b(i) could be associated with C–O–H bond vibration or solvation [32, 33]. According to Vicentini et al. [33], the band at around 1,015 cm^{-1} in starch spectrum is characteristic of amorphous material. As glycerol content increases to 30 wt%, the peak shifts to higher wavenumber of 1,017 cm^{-1} as shown in Fig. 3b(iv). Bergo et al. [32] also observed that the peak at 1,011.8 cm^{-1} in the spectrum of unplasticized starch film has shifted to higher wavenumbers with the increase in glycerol content.

Conductivity at room temperature

Conductivity at room temperature for salted system is depicted in Fig. 4a. It is observed that the ionic conductivity achieves the maximum value of $(5.57\pm1.88)\times10^{-5}$ S cm^{-1} with incorporation of 30 wt% NH_4Br. The increase in conductivity as salt concentration increases to 30 wt% can be attributed to the increase in number of charge carriers [12, 13]. As more than 30 wt% NH_4Br are added to the electrolyte, the conductivity is observed to decrease. When too much ions are provided, the possibility of ion recombination to become neutral ion pair increases which decrease the number of free mobile ions [13]. Furthermore, the formation of ion aggregates blocks the movement of the free mobile ions [34]. These phenomena decrease the conductivity. The room temperature conductivity for plasticized system is shown in Fig. 4b. Glycerol was chosen as plasticizer because glycerol was reported to be a good plasticizing agent for starch based film [35]. The addition of 30 wt% glycerol enhances the conductivity to $(1.80\pm0.26)\times10^{-3}$ S cm^{-1}. Glycerol has high dielectric constant value ($\varepsilon_{glycerol}$=42.5) which weaken the Coulombic force between the cations and anions of salt. Hence, more undissociated salt become ions to assist the conductivity enhancement. The addition of more than 30 wt% glycerol decreases the conductivity of the electrolyte. This is attributed to the formation of linkages between the plasticizer itself and causing it to recrystallize resulting in the decrease in conductivity [36].

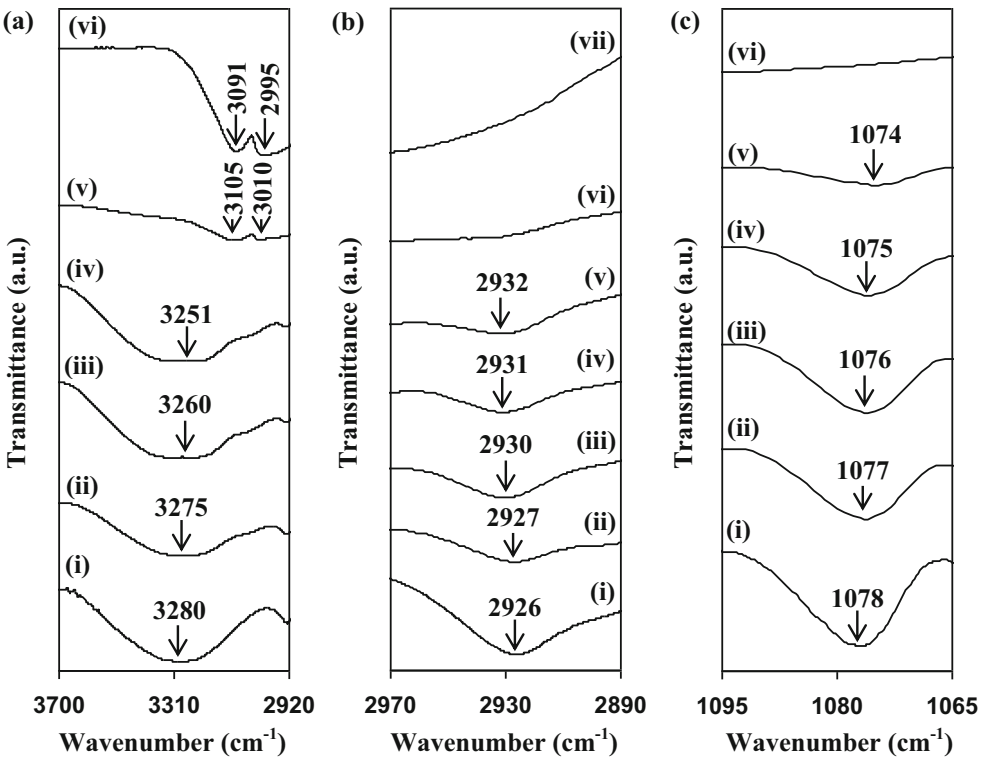

Fig. 2 **a** FTIR spectra for electrolytes comprise of *i* pure starch film, *ii* 90 wt% starch–10 wt% NH_4Br, *iii* 75 wt% starch–25 wt% NH_4Br, *iv* 70 wt% starch–30 wt% NH_4Br, *v* 60 wt% starch–40 wt% NH_4Br, and *vi* pure NH_4Br salt powder in the region of 2,920–3,700 cm^{-1}. **b** FTIR spectra for electrolytes comprise of *i* pure starch film, *ii* 85 wt% starch–15 wt% NH_4Br, *iii* 80 wt% starch–20 wt% NH_4Br, *iv* 70 wt% starch–30 wt% NH_4Br, *v* 65 wt% starch–35 wt% NH_4Br, *vi* 60 wt% starch–40 wt% NH_4Br, and *vii* pure NH_4Br salt powder in the region of 2,890–2,970 cm^{-1}. **c** FTIR spectra for electrolytes comprise of *i* pure starch film, *ii* 75 wt% starch–25 wt% NH_4Br, *iii* 70 wt% starch–30 wt% NH_4Br, *iv* 65 wt% starch–35 wt% NH_4Br, *v* 60 wt% starch–40 wt% NH_4Br, and *vi* pure NH_4Br salt powder in the region of 1,065–1,095 cm^{-1}

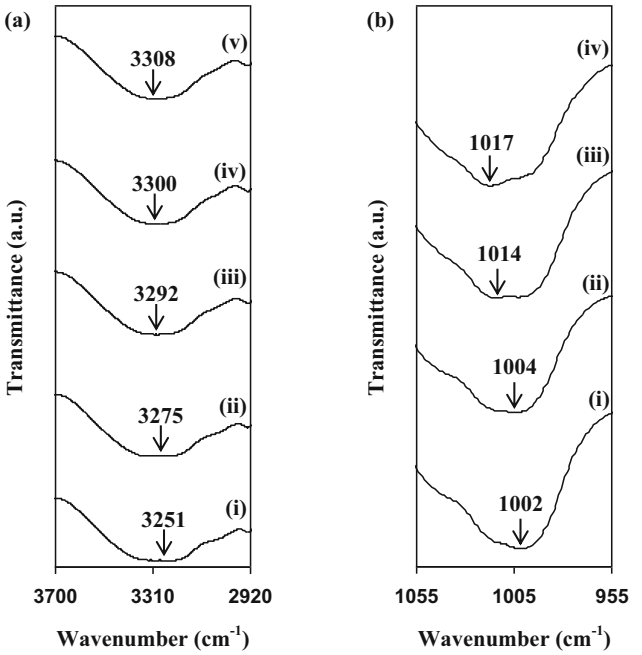

Fig. 3 **a** FTIR spectra for electrolytes comprise of *i* 70 wt% starch–30 wt% NH_4Br–0 wt% glycerol, *ii* 63 wt% starch–27 wt% NH_4Br–10 wt% glycerol, *iii* 56 wt% starch–24 wt% NH_4Br–20 wt% glycerol, *iv* 52.5 wt% starch–22.5 wt% NH_4Br–25 wt% glycerol, and *v* 49 wt% starch–21 wt% NH_4Br–30 wt% glycerol in the region of 2,920–3,700 cm^{-1}. **b** FTIR spectra for electrolytes comprise of *i* 70 wt% starch–30 wt% NH_4Br–0 wt% glycerol, *ii* 66.5 wt% starch–28.5 wt% NH_4Br–5 wt% glycerol, *iii* 63 wt% starch–27 wt% NH_4Br–10 wt% glycerol, and *iv* 49 wt% starch–21 wt% NH_4Br–30 wt% glycerol in the region of 955–1,055 cm^{-1}

Conductivity at elevated temperature

Conductivity of SPE depends strongly on the temperature. Figure 5 shows the effect of temperature on conductivity for salted and plasticized systems. It is found that the conductivity increases with temperature for all electrolytes which follows Arrhenius rule. It can be assumed that the transport of cation is quite similar to that occurring in ionic crystals, where ions jump into neighboring vacant sites [37]. Similar behavior has been reported for other polymer electrolyte systems [36–38]. Hence, the conductivity can be expressed as:

$$\sigma = \sigma_o \exp\left[-\frac{E_a}{kT}\right] \quad (5)$$

where σ_o is the pre-exponential factor, E_a is the activation energy, k is the Boltzmann constant, and T is the absolute temperature. The activation energy can be ascribed as the combination of energy of defect formation and energy of defect migration [39]. In the present work, the activation energies were evaluated from the plots in Fig. 5 and tabulated in Tables 1 and 2. For the salted system, 70 wt% starch–30 wt% NH_4Br electrolyte has the lowest activation energy of 0.56 eV while 49 wt% starch–21 wt% NH_4Br–30 wt% glycerol electrolyte has the lowest activation energy of 0.11 eV for the plasticized system. It can be inferred that the higher conducting electrolyte requires lower activation energy. Polymer electrolytes are the mixture of crystalline and amorphous regions and the conductivity behavior of such electrolytes may be dominated by the properties of the amorphous region [40]. The addition of salt forms charge transfer complexes in the host lattice which increases the conductivity by providing additional charges in the lattice resulting a decrease in activation energy [40, 41].

XRD analysis

The variation of conductivity with salt or plasticizer concentration can be verified by the XRD analysis, where the conductivity trend can be related to the amorphousness of the electrolytes. Three crystalline peaks are observed at 2θ=17.3, 19.9, and 21.9 ° in the x-ray diffractogram of pure starch film as shown in Fig. 6a. The presence of both sharp and diffuse diffraction peaks in its diffractogram demonstrates that the pure starch film shows two phase morphology, i.e., crystalline and amorphous states. The amorphousness of the starch film increases with the incorporation of 5 and 15 wt% NH_4Br, as the degree of crystallinity decreases as shown in Table 3. As ion concentration in the electrolytes increases, both fractions of amorphous phase and charge carriers increased simultaneously [42]. The intensity of the three crystalline peaks of pure starch film decreases as shown in Fig. 6b, c, which proves that the addition of salt decreases the crystalline phase of the electrolyte. On addition of 30 wt% NH_4Br, the crystalline peaks disappear as shown in Fig. 6d and the degree of crystallinity further decreases. Since ions are preferably mobile in the amorphous phase, these results explain the increasing conductivity value with increasing NH_4Br content up to 30 wt%. The presence of glycerol in the electrolyte further increases the amorphousness of the electrolytes. From Fig. 4b, the conductivity is maximized with addition of 30 wt% glycerol. From Table 3, 49 wt% starch–21 wt% NH_4Br–30 wt% glycerol electrolyte has the lowest value of the degree of crystallinity, indicating that the electrolyte has the highest amorphous content which is consistent with the conductivity result.

Impedance analysis

A typical AC impedance plot consists of a semicircle curve at the high-frequency region and a tilted spike at the low-frequency region. The semicircle part is related to ionic conduction in the bulk of the sample [38]. According to Malathi et al. [43], the bulk conductivity is due to the parallel combination of bulk resistance and bulk capacitance of the polymer electrolytes. The tilted spike is attributed to the effect of electrode polarization which is characteristic of the diffusion

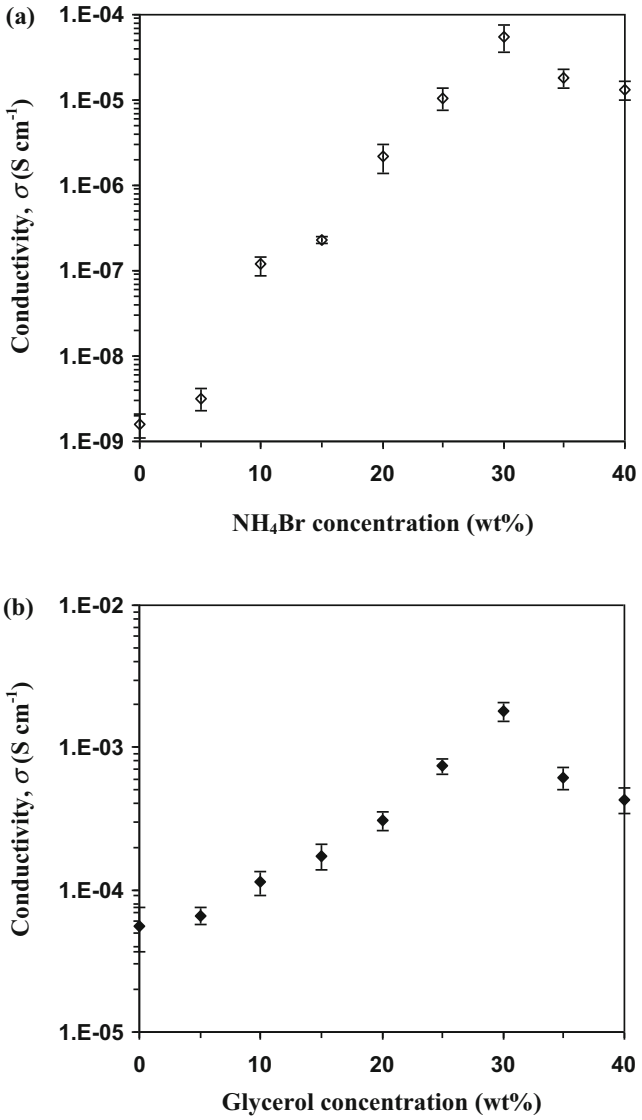

Fig. 4 Conductivity at room temperature for **a** salted system and **b** plasticized system

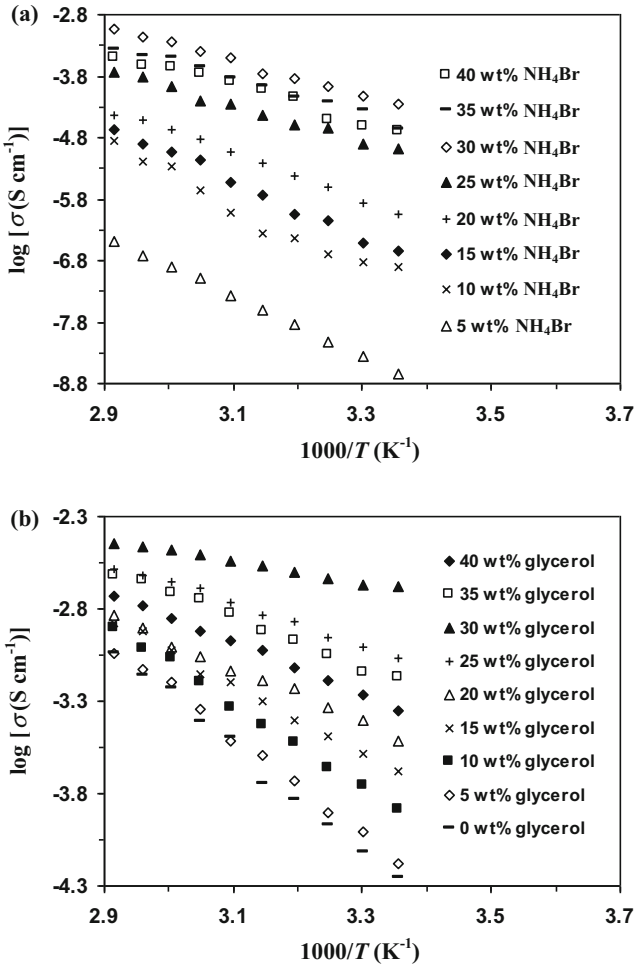

Fig. 5 Conductivity at elevated temperature for **a** salted system and **b** plasticized system

process [38]. Figure 7 shows the Nyquist plots of 49 wt% starch–21 wt% NH_4Br–30 wt% glycerol electrolyte at various temperatures. It is observed that the Nyquist plot for each temperature consists of only a tilted spike. The disappearance of semicircle at high-frequency region suggests that only the resistive component of the polymer prevails [17]. The tilted spikes inclined at an angle less than 90 ° with the real axis. According to Wu et al. [44], the inclination of the spike at an angle less than 90 ° with the real axis is attributed to the non-homogeneous or roughness of the electrode-electrolyte interface.

The electrical equivalent circuit representation is commonly used in impedance analysis because it is fast, simple, and provides the complete picture of the system [45]. In the present work, since the Nyquist plot of 49 wt% starch–21 wt% NH_4Br–30 wt% glycerol electrolyte at all temperatures consists only the tilted spike; the equivalent circuit can be represented by a combination of R_b and constant phase element (CPE) in series [46]. In general, a CPE is used in a model instead of a capacitor to compensate for inhomogeneity in the system [47]. The impedance of CPE (Z_{CPE}) can be expressed as [46, 48]:

Table 1 Conductivity and E_a values for salted system

Sample (wt% NH_4Br)	σ (S cm^{-1})	E_a (eV)
5	$(3.18\pm0.91)\times10^{-9}$	0.97
10	$(1.18\pm0.30)\times10^{-7}$	0.96
15	$(2.27\pm0.23)\times10^{-7}$	0.93
20	$(2.18\pm0.80)\times10^{-6}$	0.76
25	$(1.07\pm0.30)\times10^{-5}$	0.58
30	$(5.57\pm1.88)\times10^{-5}$	0.56
35	$(1.82\pm0.44)\times10^{-5}$	0.57
40	$(1.32\pm0.32)\times10^{-5}$	0.57

Table 2 Conductivity and E_a values for plasticized system

Sample (wt% glycerol)	σ (S cm^{-1})	E_a (eV)
5	$(6.54\pm0.90)\times10^{-5}$	0.52
10	$(1.13\pm0.22)\times10^{-4}$	0.44
15	$(1.74\pm0.35)\times10^{-4}$	0.37
20	$(3.04\pm0.45)\times10^{-4}$	0.29
25	$(7.41\pm1.00)\times10^{-4}$	0.23
30	$(1.80\pm0.26)\times10^{-3}$	0.11
35	$(6.17\pm1.06)\times10^{-4}$	0.27
40	$(4.34\pm0.87)\times10^{-4}$	0.28

$$Z_{\mathrm{CPE}} = \frac{1}{C\omega^{p}}\left[\cos\left(\frac{\pi p}{2}\right) - i\ \sin\left(\frac{\pi p}{2}\right)\right] \tag{6}$$

where C is the capacitance of CPE and p is related to the deviation of the plot from the axis. The values of Z_r and Z_i associated to the equivalent circuit can be expressed as:

$$Z_r = R + \frac{\cos\left(\frac{\pi p}{2}\right)}{C\omega^{p}} \tag{7}$$

$$Z_i = \frac{\sin\left(\frac{\pi p}{2}\right)}{C\omega^{p}} \tag{8}$$

The parameters of the circuit elements at various temperatures are tabulated in Table 4. The value of capacitance is observed to increase with increasing temperature. According to Shuhaimi et al. [46], the increase in capacitance with increasing temperature implies the suitability for the use in electrochemical devices. The

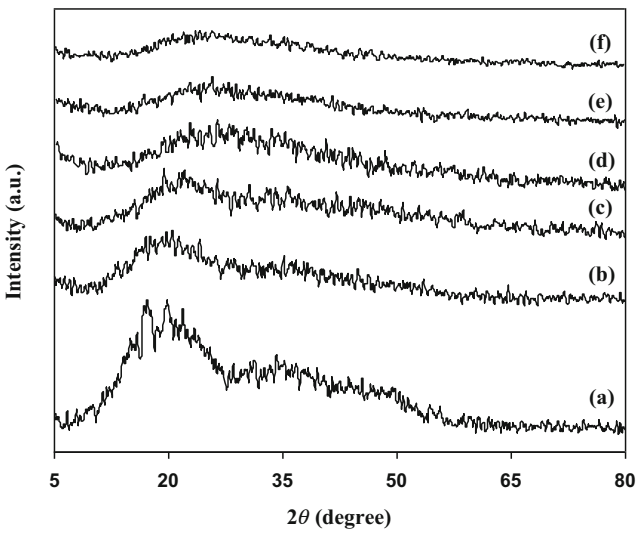

Fig. 6 X-ray diffractograms of **a** pure starch film, **b** 95 wt% starch–5 wt% NH_4Br, **c** 85 wt% starch–15 wt% NH_4Br, **d** 70 wt% starch–30 wt% NH_4Br, **e** 63 wt% starch–27 wt% NH_4Br–10 wt% glycerol, and **f** 49 wt% starch–21 wt% NH_4Br–30 wt% glycerol electrolytes

Table 3 Degree of crystallinity of selected electrolyte samples

Electrolyte	χ_c (%)
Pure starch	30.36
95 wt% starch–5 wt% NH_4Br	28.80
85 wt% starch–15 wt% NH_4Br	26.23
70 wt% starch–30 wt% NH_4Br	25.57
63 wt% starch–27 wt% NH_4Br–10 wt% glycerol	25.44
49 wt% starch–21 wt% NH_4Br–30 wt% glycerol	22.42

increasing capacitance with increasing temperature satisfies the following equation:

$$C = \frac{\varepsilon_o \varepsilon_r A}{t} \tag{9}$$

where ε_o is vacuum permittivity. Many reports [26, 37, 48] have shown that the value of the ε_r of a polymer electrolyte increases with increasing temperature, which in turn, increases the capacitance. The result of ε_r in this work will be discussed later.

Dielectric analysis

Dielectric constant is representative of stored charge in a material while dielectric loss is a measure of energy losses to move ions when the polarity of electric field reverses rapidly [18, 26]. The frequency dependence of ε_r and ε_i for 70 wt% starch–30 wt% NH_4Br electrolyte and 49 wt% starch–21 wt% NH_4Br–30 wt% glycerol electrolyte from 298 to 343 K are shown in Figs. 8 and 9, respectively. No relaxation peaks are observed indicating that the increase in conductivity is mainly due to the increase in number density of mobile ions [12]. As the temperature increases, the values of ε_r and ε_i increase due to the total polarization that arises from the dipole orientation and the trapped charge carriers [49]. As reported by Ramesh et al. [37], the plasticized electrolyte with higher conductivity value shows much higher ε_r value. The higher ε_r and ε_i values obtained by 49 wt% starch–21 wt% NH_4Br–30 wt% glycerol electrolyte at low-frequency region indicates that the existence of plasticizer may result in more localization of charge carriers along with mobile ions causing higher ionic conductivity [50].

The decreasing ε_r and ε_i with increasing frequency is attributed to the tendency of the dipoles in the polymer chains to orient themselves in the direction of the applied electric field [49]. Towards higher frequencies, the fast periodic reversal of the electric field occurs hence the polarization due to charge accumulation decreases at the electrode–electrolyte interface, which in turn,

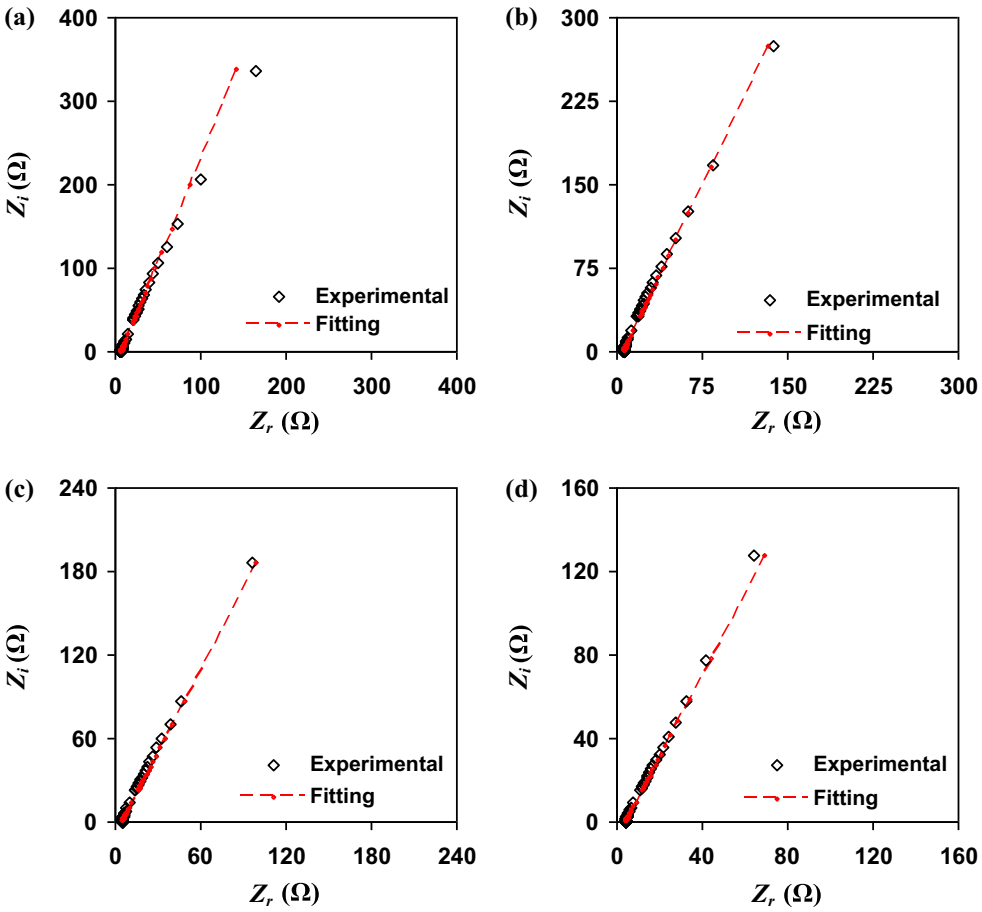

Fig. 7 Nyquist plot of 49 wt% starch-21 wt% NH_4Br-30 wt% glycerol electrolyte at **a** 298 K, **b** 313 K, **c** 328 K, and **d** 343 K

contributes to the decrease in ε_r and ε_i [37]. Dielectric results imply that the electrolyte systems in the present work confirm the non-Debye behavior.

Conduction mechanism

The AC conductivity (σ_{AC}) is obtained using:

$$\sigma_{AC} = \varepsilon_o \varepsilon_r \omega \tan\delta \tag{10}$$

Table 4 The parameters of the circuit elements for 49 wt% starch–21 wt%

T (K)	p (rad)	C (F)
298	0.76	3.51×10^{-5}
303	0.74	4.00×10^{-5}
308	0.72	4.74×10^{-5}
313	0.72	5.13×10^{-5}
318	0.71	6.25×10^{-5}
323	0.71	6.80×10^{-5}
328	0.70	8.47×10^{-5}
333	0.70	9.62×10^{-5}
338	0.70	1.09×10^{-4}
343	0.70	1.26×10^{-4}

By substituting $\varepsilon_r \tan\delta = \varepsilon_i$ into Eq. (10):

$$\sigma_{AC} = \varepsilon_o \varepsilon_i \omega \tag{11}$$

According to Jonscher's universal power law [51], the total conductivity ($\sigma(\omega)$) is the sum of σ_{AC} and DC conductivity (σ_{DC}).

$$\sigma(\omega) = \sigma_{AC} + \sigma_{DC} \tag{12}$$

$$\sigma(\omega) = A\omega^s + \sigma_{DC} \tag{13}$$

Here, $A\omega^s = \sigma_{AC}$. A represents a parameter dependent on temperature and s is the power law exponent with $0<s<1$. By substituting $A\omega^s = \sigma_{AC}$ into Eq. (11), the value of s was obtained by plotting Eq. (14).

$$\ln\varepsilon_i = \ln\frac{A}{\varepsilon_o} + (s-1)\ln\omega \tag{14}$$

The value of s was determined from the slope of the plots in Fig. 10. In the present work, the slope is only taken in the frequency range of $12.3<\ln\omega<13.0$ since there is no or minimal impact of electrode polarization at high-frequency region [26]. At a higher frequency region, most of the ions are

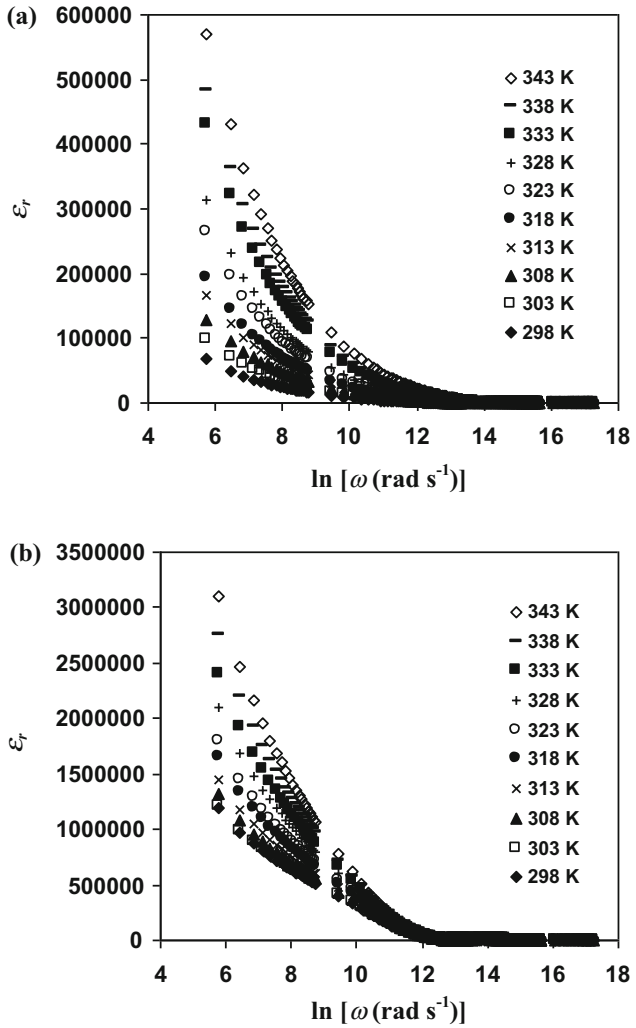

Fig. 8 Frequency dependence of dielectric constant at different temperatures for **a** 70 wt% starch–30 wt% NH_4Br electrolyte and **b** 49 wt% starch–21 wt% NH_4Br–30 wt% glycerol electrolyte

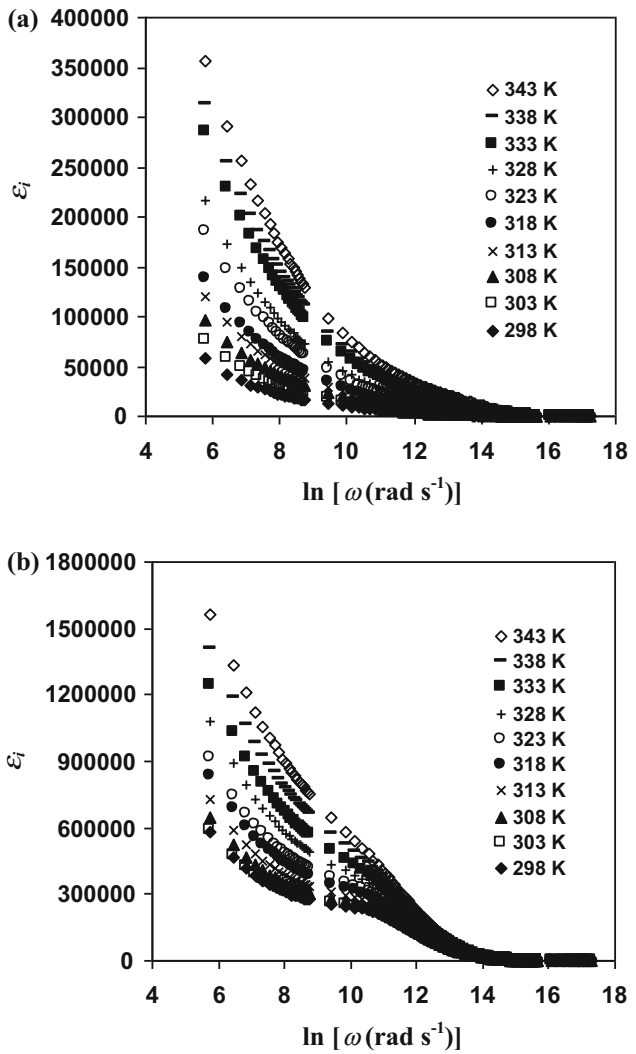

Fig. 9 Frequency dependence of dielectric loss at different temperatures for **a** 70 wt% starch–30 wt% NH_4Br electrolyte and **b** 49 wt% starch–21 wt% NH_4Br–30 wt% glycerol electrolyte

static as the periodic reversal of electric field occurs so fast, hence, decreasing the electrode polarization. There are a lot of reports which suggest that the acceptable frequency range is outside of the electrode polarization region [26, 52]. Figure 11 shows the variation of s with temperature for 70 wt% starch–30 wt% NH_4Br electrolyte and 49 wt% starch–21 wt% NH_4Br–30 wt% glycerol electrolyte. For 70 wt% starch–30 wt% NH_4Br electrolyte, the value of s decreases towards 308 K and increases thereafter. This may be due to the breaking of internal correlation between the sites and relaxing ions and relaxing species become independent of each other which results in tunneling process rather than hopping [53]. This result infers that the conduction mechanism of 70 wt% starch–30 wt% NH_4Br electrolyte can be explained by the overlapping large polaron tunneling (OLPT) model [54]. The plot of s against temperature for 49 wt% starch–21 wt% NH_4Br–30 wt% glycerol electrolyte shows a decreasing value with increasing temperature and is best fitted by the equation of $s=-0.0027\ T+0.948$, where as $T\rightarrow 0$ K, the exponent s is approaching ~1. This result implies that the conduction mechanism of the electrolyte follows the correlated barrier hopping (CBH) model [55]. Buraidah et al. [26] reported that the conduction mechanism for chitosan–NH_4I occurs by way of CBH model in which the plot of exponent s against T can be fitted to the equation $s=-0.0023\ T+1.0281$. Their result is comparable with the present work. In this model, the ions reside in a potential well. The ions are assumed to be surrounded by several potentials such as the Columbic repulsive potential between the ions and the potential well. The ions can hop from one site to another after they acquired enough energy. The ions may hop back to the initial site or the formation of a new absolute potential with an increase in the back-hop barrier height and the ions continue to move in the forward direction [26]. The hops are thermally activated. According to Kufian et al. [56], the difference in conduction

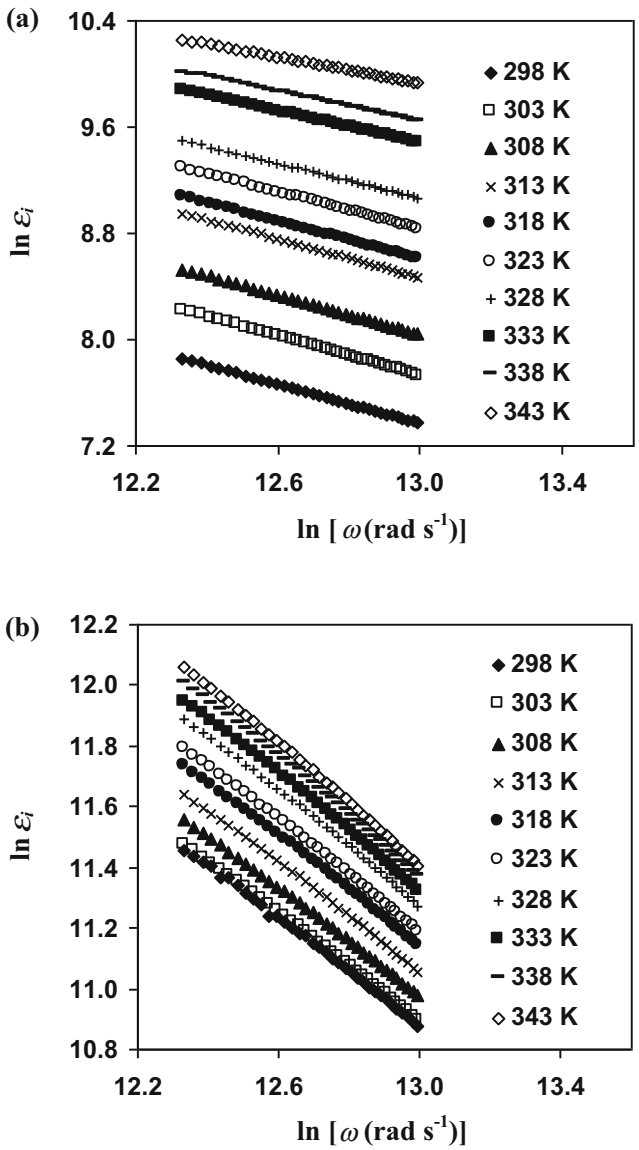

Fig. 10 Variation of ln ε_i with frequency at different temperatures for **a** 70 wt% starch–30 wt% NH_4Br electrolyte and **b** 49 wt% starch–21 wt% NH_4Br–30 wt% glycerol electrolyte

mechanism can be attributed to the different E_a value of the electrolytes. The E_a for 70 wt% starch–30 wt% NH_4Br electrolyte is 0.56 eV. Due to the higher E_a, the ions prefer to tunnel through the potential barrier rather than hop across it. For 49 wt% starch–21 wt% NH_4Br–30 wt% glycerol electrolyte, the E_a is lower. Hence, the ions can easily hop across the potential barrier giving rise to a higher conductivity.

Transference number analysis

The contribution of ions to the total conductivity of an electrolyte can be determined from the transference number measurement [57]. From the plot of polarization current against time in Fig. 12a, the transference numbers of ion (t_{ion}) and electron (t_e) for 49 wt% starch–21 wt% NH_4Br–30 wt% glycerol electrolyte were calculated using:

$$t_{ion} = \frac{I_i - I_{ss}}{I_i} \tag{15}$$

$$t_e = \frac{I_{ss}}{I_i} \tag{16}$$

where I_i is the initial current and I_{ss} is the steady state current. The steady state is achieved when the movement of mobile ions is balanced by diffusion process, which is due to the ion concentration gradient [58]. The concentration gradient is ascribed to the non unity transference number of ions in the polymer electrolyte which causes decay in current to lower steady state value [59]. It is found that t_{ion} is 0.98 and t_e is 0.02, indicating that the charge transport in the polymer complex is predominantly due to ions. Hema et al. [17] reported t_{ion} for all the compositions of the PVA-NH_4Br electrolyte system lies between 0.93 and 0.96 at room temperature. The ionic transference number for potato starch–ammonium iodide (NH_4I) electrolyte is reported to be >0.95 [60]. The results from the literature are comparable with the present work.

Proton transference number (t_p) for 49 wt% starch–21 wt% NH_4Br–30 wt% glycerol electrolyte was determined using Watanabe's method. The value of t_p was calculated using:

$$t_p = \frac{R_b}{\frac{\Delta V}{I_{ss}} - R_c} \tag{17}$$

where ΔV is the bias voltage from DC polarization and R_c is the charge transfer resistance. The phenomenon of R_c is attributed to the charging–discharging electrode–electrolyte interface [58]. In this technique, the values of R_b and R_c were measured from a complex impedance plot using non-blocking reversible MnO_2 electrodes. Figure 12b shows the plot of polarization current against time at applied voltage of 0.20 V using MnO_2 electrodes. It is found that I_{ss} is 28.0 μA. The impedance plot for MnO_2/49 wt% starch–21 wt% NH_4Br–30 wt% glycerol electrolyte/MnO_2 cell is depicted in Fig. 13. Using the obtained values of R_b and R_c, the t_p value is then evaluated. The value of I_{ss} must be taken from the region in which the I_{ss} vs V plot is linear [58, 59]. Such plot is depicted inset of Fig. 13. The value of t_p is found to be 0.35. According to Watanabe and Nishimoto [61], although the transference number is affected by the phenomenon of ionic association, it may still offer an insight into the ion transport process. Other reports show that the cation transference numbers range from 0.21 to 0.46 at ambient temperature [58, 59, 62].

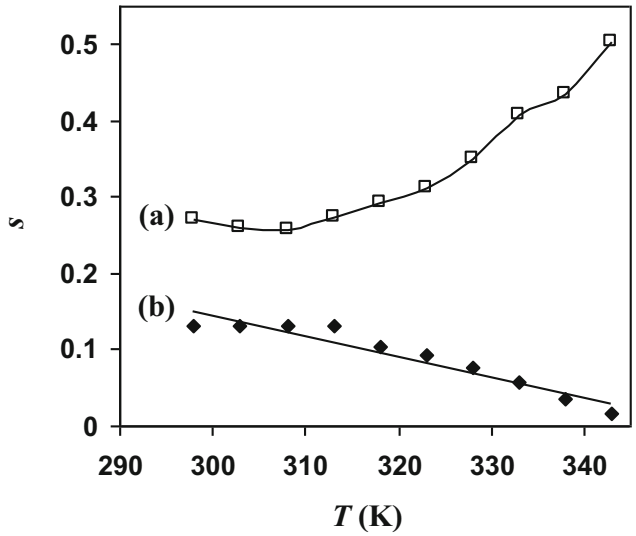

Fig. 11 Variation of *s* with temperature for **a** 70 wt% starch–30 wt% NH_4Br electrolyte and **b** 49 wt% starch–21 wt% NH_4Br–30 wt% glycerol electrolyte

Electrochemical stability window

LSV measurement was carried out in order to determine the stability window of the electrolyte as well as the maximum operational voltage of an electrochemical device employing the electrolyte [63]. The corresponding voltammogram is shown in Fig. 14. It can be observed that the decomposition voltage of 49 wt% starch–21 wt% NH_4Br–30 wt% glycerol electrolyte is 1.66 V. According to Pratap et al. [14], the standard electrochemical window of proton batteries is ~1 V. Arof et al. [57] reported that the decomposition voltage of PMMA-LiBOB electrolyte is 1.7 V and the electrolyte was used in fabrication of an electrical double layer capacitor (EDLC). The present result shows that 49 wt% starch–21 wt% NH_4Br–30 wt% glycerol electrolyte is suitable for fabrication of electrochemical devices.

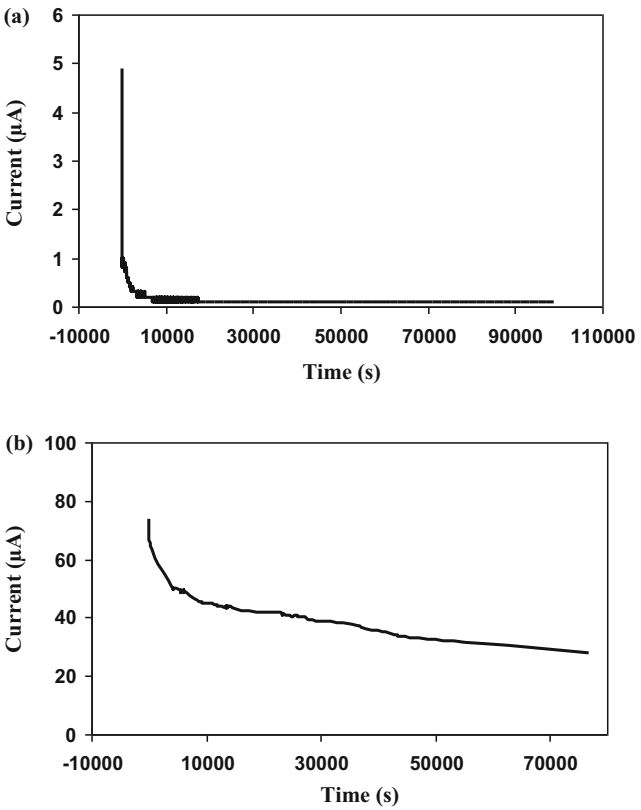

Fig. 12 Transference number of 49 wt% starch–21 wt% NH_4Br–30 wt% glycerol electrolyte at room temperature using **a** stainless steel electrodes and **b** MnO_2 electrodes

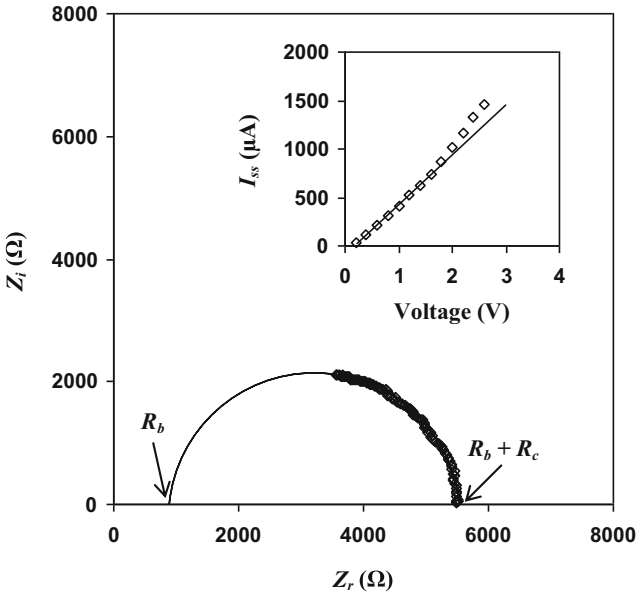

Fig. 13 Impedance plot for MnO_2/49 wt% starch–21 wt% NH_4Br–30 wt% glycerol electrolyte/MnO_2 cell at room temperature. Inset is I_{ss} as a function of voltage at room temperature

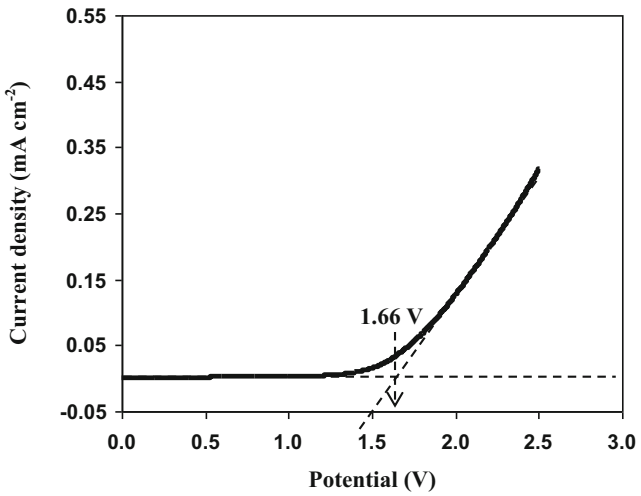

Fig. 14 Linear sweep voltammogram for 49 wt% starch–21 wt% NH_4Br–30 wt% glycerol electrolyte at 10 mV s^{-1}

Conclusions

Polymer electrolytes based on corn starch and doped with NH_4Br have been prepared by solution casting technique. From FTIR results, the shifting of hydroxyl, C–H stretching mode, and C–O bond stretching bands of pure starch film prove the interaction between starch and NH_4Br salt. The peak at 1,002 cm^{-1} in the spectrum of 70 wt% starch–30 wt% NH_4Br electrolyte, as well as the hydroxyl band, shifts to higher wavenumbers with the increase in glycerol content. For the salted system, 70 wt% starch–30 wt% NH_4Br electrolyte exhibits the highest room temperature conductivity of $(5.57\pm1.88)\times10^{-5}$ S cm^{-1}. For the plasticized system, 49 wt% starch–21 wt% NH_4Br–30 wt% glycerol electrolyte exhibits the highest room temperature conductivity of $(1.80\pm0.26)\times10^{-3}$ S cm^{-1}. The temperature dependence of ionic conductivity for all electrolytes exhibits Arrhenius behavior and the activation energy values decreases with increasing conductivity. XRD results verify the conductivity result. Dielectric results imply that the electrolyte systems in the present work confirm the non-Debye behavior. The conduction mechanism of 70 wt% starch–30 wt% NH_4Br electrolyte follows the OLPT model and 49 wt% starch–21 wt% NH_4Br–30 wt% glycerol electrolyte follows the CBH model. The ionic and protonic transference numbers of 49 wt% starch–21 wt% NH_4Br–30 wt% glycerol electrolyte are 0.98 and 0.35, respectively. LSV analysis shows that 49 wt% starch–21 wt% NH_4Br–30 wt% glycerol electrolyte is suitable for devices application.

Acknowledgments The authors would like to thank the University of Malaya for the financial support (Grant no. PG046-2013A).

References

1. Takami N, Sekino M, Ohsaki T, Kanda M, Yamamoto M (2001) New thin lithium-ion batteries using a liquid electrolyte with thermal stability. J Power Sources 97–98:677–680. doi:10.1016/S0378-7753(01)00699-1
2. Hofmann A, Schulz M, Hanemann T (2013) Gel electrolytes based on ionic liquids for advanced lithium polymer batteries. Electrochim Acta 89:823–831. doi:10.1016/j.electacta.2012.10.144
3. Deepa M, Sharma N, Agnihotry SA, Singh S, Lal T, Chandra R (2002) Conductivity and viscosity of liquid and gel electrolytes based on $LiClO_4$, $LiN(CF_3SO_2)_2$ and PMMA. Solid State Ionics 152–153: 253–258. doi:10.1016/S0167-2738(02)00307-7
4. Perera K, Dissanayake MAKL (2006) Conductivity variation of the liquid electrolyte, EC : PC : $LiCF_3SO_3$ with salt concentration. Sri Lankan J Phys 7:1–5. doi:10.4038/sljp.v7i0.202
5. Lee CP, Chen PY, Vittal R, Ho KC (2010) Iodine-free high efficient quasi solid-state dye-sensitized solar cell containing ionic liquid and polyaniline-loaded carbon black. J Mater Chem 20:2356–2361. doi:10.1039/B922350A
6. Lee CP, Lin LY, Chen PY, Vittal R, Ho KC (2010) All-solid-state dye-sensitized solar cells incorporating SWCNTs and crystal growth inhibitor. J Mater Chem 20:3619–3625. doi:10.1039/B925221E
7. Ramesh S, Liew CW, Arof AK (2011) Ion conducting corn starch biopolymer electrolytes doped with ionic liquid 1-butyl-3-methylimidazolium hexafluorophosphate. J Non-Cryst Solids 357:3654–3660. doi:10.1016/j.jnoncrysol.2011.06.030
8. Ma X, Yu J, He K, Wang N (2007) The effects of different plasticizers on the properties of thermoplastic starch as solid polymer electrolytes. Macromol Mater Eng 292:503–510. doi:10.1002/mame.200600445
9. Lu DR, Xiao CM, Xu SJ (2009) Starch-based completely biodegradable polymer materials. Express Polym Lett 3:366–375. doi:10.3144/expresspolymlett.2009.46
10. Varshney PK, Gupta S (2011) Natural polymer-based electrolytes for electrochemical devices: a review. Ionics 17:479–483. doi:10.1007/s11581-011-0563-1
11. Marcondes RFMS, D'Agostini PS, Ferreira J, Girotto EM, Pawlicka A, Dragunski DC (2010) Amylopectin-rich starch plasticized with glycerol for polymer electrolyte application. Solid State Ionics 181: 586–591. doi:10.1016/j.ssi.2010.03.016
12. Khiar ASA, Arof AK (2010) Conductivity studies of starch-based polymer electrolytes. Ionics 16:123–129. doi:10.1007/s11581-009-0356-y
13. Kadir MFZ, Majid SR, Arof AK (2010) Plasticized chitosan-PVA blend polymer electrolyte based proton battery. Electrochim Acta 55: 1475–1482. doi:10.1016/j.electacta.2009.05.011
14. Pratap R, Singh B, Chandra S (2006) Polymeric rechargeable solid-state proton battery. J Power Sources 161:702–706. doi:10.1016/j.jpowsour.2006.04.020
15. Prajapati GK, Roshan R, Gupta PN (2010) Effect of plasticizer on ionic transport and dielectric properties of PVA-H_3PO_4 proton conducting polymeric electrolytes. J Phys Chem Solids 71:1717–1723. doi:10.1016/j.jpcs.2010.08.023
16. Raj CJ, Varma KBR (2010) Synthesis and electrical properties of the $(PVA)_{0.7}(KI)_{0.3}\cdot xH_2SO_4$ $(0\le x\le5)$ polymer electrolytes and their performance in a primary Zn/MnO_2 battery. Electrochim Acta 56:649–656. doi:10.1016/j.electacta.2010.09.076
17. Hema M, Selvasekerapandian S, Sakunthala A, Arunkumar D, Nithya H (2008) Structural, vibrational and electrical characterization of PVA-NH_4Br polymer electrolyte system. Physica B 403:2740–2747. doi:10.1016/j.physb.2008.02.001
18. Woo HJ, Majid SR, Arof AK (2012) Dielectric properties and morphology of polymer electrolyte based on poly(ε-caprolactone) and ammonium thiocyanate. Mater Chem Phys 134:755–761. doi:10.1016/j.matchemphys.2012.03.064
19. Kadir MFZ, Aspanut Z, Majid SR, Arof AK (2011) FTIR studies of plasticized poly(vinyl alcohol)-chitosan blend doped with NH_4NO_3 polymer electrolyte membrane. Spectrochim Acta A 78:1068–1074. doi:10.1016/j.saa.2010.12.051
20. Vijaya N, Selvasekarapandian S, Hirankumar G, Karthikeyan S, Nithya H, Ramya CS, Prabu M (2012) Structural, vibrational, thermal, and conductivity studies on proton-conducting polymer electrolyte based on poly(*N*-vinylpyrrolidone). Ionics 18:91–99. doi:10.1007/s11581-011-0589-4
21. Wagner JB, Wagner CJ (1957) Electrical conductivity measurements on cuprous halides. J Chem Phys 26:1597–1601. doi:10.1063/1.1743590
22. Watanabe M, Nagano S, Sanui K, Ogata N (1988) Estimation of Li^+ transport number in polymer electrolytes by the combination of complex impedance and potentiostatic polarization measurements. Solid State Ionics 28–30:911–917. doi:10.1016/0167-2738(88)90303-7
23. Hema M, Selvasekarapandian S, Nithya H, Sakunthala A, Arunkumar D (2009) FTIR, XRD and ac impedance spectroscopic study on PVA based polymer electrolyte doped with NH_4X (X=Cl, Br, I). J Non-Cryst Solids 355:84–90. doi:10.1016/j.jnoncrysol.2008.10.009

24. Teoh KH, Ramesh S, Arof AK (2012) Investigation on the effect of nanosilica towards corn starch-lithium perchlorate-based polymer electrolytes. J Solid State Electrochem 16:3165–3170. doi:10.1007/s10008-012-1741-4
25. Shukur MF, Ithnin R, Illias HA, Kadir MFZ (2013) Proton conducting polymer electrolyte based on plasticized chitosan-PEO blend and application in electrochemical devices. Opt Mater 35:1834–1841. doi:10.1016/j.optmat.2013.03.004
26. Buraidah MH, Teo LP, Majid SR, Arof AK (2009) Ionic conductivity by correlated barrier hopping in NH_4I doped chitosan solid electrolyte. Physica B 404:1373–1379. doi:10.1016/j.physb.2008.12.027
27. Stygar J, Zukowska G, Wieczorek W (2005) Study of association in alkali metal perchlorate-poly(ethylene glycol) monomethyl ether solutions by FT-IR spectroscopy and conductivity measurements. Solid State Ionics 176:2645–2652. doi:10.1016/j.ssi.2005.07.006
28. Ning W, Xingxiang Z, Haihui L, Benqiao H (2009) 1-Allyl-3-methylimidazolium chloride plasticized-corn starch as solid biopolymer electrolytes. Carbohydr Polym 76:482–484. doi:10.1016/j.carbpol.2008.11.005
29. Liang S, Huang Q, Liu L, Yam KL (2009) Microstructure and molecular interaction in glycerol plasticized chitosan/poly(vinyl alcohol) blending films. Macromol Chem Phys 210:832–839. doi:10.1002/macp.200900053
30. Shukur MF, Ibrahim F, Majid NA, Ithnin R, Kadir MFZ (2013) Electrical analysis of amorphous corn starch-based polymer electrolyte membranes doped with LiI. Phys Scr 88:025601. doi:10.1088/0031-8949/88/02/025601
31. Liu H, Adhikari R, Guo Q, Adhikari B (2013) Preparation and characterization of glycerol plasticized (high-amylose) starch-chitosan films. J Food Eng 116:588–597. doi:10.1016/j.jfoodeng.2012.12.037
32. Bergo PVA, Sobral PJA, Prison JM (2009) Physical properties of cassava starch films containing glycerol. Gene Conserve 8:727–734
33. Vicentini NM, Dupuy N, Leitzelman M, Cereda MP, Sobral PJA (2005) Prediction of cassava starch eible film properties by chemometric analysis of infrared spectra. Spectrosc Lett 38:749–767. doi:10.1080/00387010500316080
34. Li M, Yang L, Fang S, Dong S (2011) Novel polymeric ionic liquid membranes as solid polymer electrolytes with high ionic conductivity at moderate temperature. J Membr Sci 366:245–250. doi:10.1016/j.memsci.2010.10.004
35. Curvelo AAS, de Carvalho AJF, Agnelli JAM (2001) Thermoplastic starch-cellulosic fibers composites: preliminary results. Carbohydr Polym 45:183–188. doi:10.1016/S0144-8617(00)00314-3
36. Johan MR, Ting LM (2011) Structural, thermal and electrical properties of nano manganese-composite polymer electrolytes. Int J Electrochem Sci 6:4737–4748
37. Ramesh S, Yahaya AH, Arof AK (2002) Dielectric behaviour of PVC-based polymer electrolytes. Solid State Ionics 152–153:291–294. doi:10.1016/S0167-2738(02)00311-9
38. Samsudin AS, Khairul WM, Isa MIN (2012) Characterization on the potential of carboxy methylcellulose for application as proton conducting biopolymer electrolytes. J Non-Cryst Solids 358:1104–1112. doi:10.1016/j.jnoncrysol.2012.02.004
39. Osman Z, Ghazali MIM, Othman L, Isa KBM (2012) AC ionic conductivity and DC polarization method of lithium ion transport in PMMA–$LiBF_4$ gel polymer electrolytes. Results Phys 2:1–4. doi:10.1016/j.rinp.2011.12.001
40. Mohan KR, Achari VBS, Rao VVRN, Sharma AK (2011) Electrical and optical properties of (PEMA/PVC) polymer blend electrolyte doped with $NaClO_4$. Polym Test 30:881–886. doi:10.1016/j.polymertesting.2011.08.010
41. Ramu C, Naidu YRV, Sharma AK (1994) Dielectric relaxation in iodine doped cellulose acetate films. Ferroelectrics 159:275–280. doi:10.1080/00150199408007585
42. Aji MP, Masturi BS, Khairurrijal AM (2012) A general formula for ion concentration-dependent electrical conductivities in polymer electrolytes. Am J Appl Sci 9:946–954. doi:10.3844/ajassp.2012.946.954
43. Malathi J, Kumaravadivel M, Brahmanandhan GM, Hema M, Baskaran R, Selvasekarapandian S (2010) Structural, thermal and electrical properties of PVA–LiCF3SO3 polymer electrolyte. J Non-Cryst Solids 356:2277–2281. doi:10.1016/j.jnoncrysol.2010.08.011
44. Wu GM, Lin SJ, Yang CC (2006) Preparation and characterization of PVA/PAA membranes for solid polymer electrolytes. J Membr Sci 275:127–133. doi:10.1016/j.memsci.2005.09.012
45. Han DG, Choi GM (1998) Computer simulation of the electrical conductivity of composites: the effect of geometrical arrangement. Solid State Ionics 106:71–87. doi:10.1016/S0167-2738(97)00484-0
46. Shuhaimi NEA, Teo LP, Woo HJ, Majid SR, Arof AK (2012) Electrical double-layer capacitors with plasticized polymer electrolyte based on methyl cellulose. Polym Bull 69:807–826. doi:10.1007/s00289-012-0763-5
47. Qian X, Gu N, Cheng Z, Yang X, Wang E, Dong S (2001) Impedance study of $(PEO)_{10}LiClO_4$–Al_2O_3 composite polymer electrolyte with blocking electrodes. Electrochim Acta 46:1829–1836. doi:10.1016/S0013-4686(00)00723-4
48. Teo LP, Buraidah MH, Nor AFM, Majid SR (2012) Conductivity and dielectric studies of Li_2SnO_3. Ionics 18:655–665. doi:10.1007/s11581-012-0667-2
49. Nithya H, Selvasekarapandian S, Kumar DA, Sakunthala A, Hema M, Christopherselvin P, Kawamura J, Baskaran R, Sanjeeviraja C (2011) Thermal and dielectric studies of polymer electrolyte based on P(ECH-EO). Mater Chem Phys 126:404–408. doi:10.1016/j.matchemphys.2010.10.047
50. Pradhan DK, Choudhary RNP, Samantaray BK (2009) Studies of dielectric and electrical properties of plasticized polymer nanocomposite electrolytes. Mater Chem Phys 115:557–561. doi:10.1016/j.matchemphys.2009.01.008
51. Jonscher AK (1996) Universal relaxation law. Chelsea Dielectrics Press, London
52. Kadir MFZA, Teo LP, Majid SR, Arof AK (2009) Conductivity studies on plasticised PEO/chitosan proton conducting polymer electrolyte. Mater Res Innov 13:259–262. doi:10.1179/143307509X440460
53. Gondaliya N, Kanchan DK, Sharma P, Joge P (2011) Structural and conductivity studies of poly(ethylene oxide)-silver triflate polymer electrolyte system. Mater Sci Appl 2:1639–1643. doi:10.4236/msa.2011.211218
54. Deen LMSE (2000) The ac conductivity studies for Cu2O–Bi_2O_3 glassy system. Mater Chem Phys 65:275–281. doi:10.1016/S0254-0584(00)00244-3
55. Winie T, Arof AK (2004) Dielectric behaviour and ac conductivity of $LiCF_3SO_3$ doped H-chitosan polymer films. Ionics 10:193–199. doi:10.1007/BF02382816
56. Kufian MZ, Majid SR, Arof AK (2007) Dielectric and conduction mechanism studies of PVA-orthophosphoric acid polymer electrolyte. Ionics 13:231–234. doi:10.1007/s11581-007-0098-7
57. Arof AK, Kufian MZ, Syukur MF, Aziz MF, Abdelrahman AE, Majid SR (2012) Electrical double layer capacitor using poly(methyl methacrylate)-C_4BO_8Li gel polymer electrolyte and carbonaceous material from shells of *mata kucing* (*Dimocarpus longan*) fruit. Electrochim Acta 74:39–45. doi:10.1016/j.electacta.2012.03.171
58. Woo HJ, Majid SR, Arof AK (2011) Transference number and structural analysis of proton conducting polymer electrolyte based on poly(ε-caprolactone). Mater Res Innov 15:S49–S54. doi:10.1179/143307511X13031890747697
59. Bhargav PB, Mohan VM, Sharma AK, Rao VVRN (2009) Investigations on electrical properties of (PVA:NaF) polymer electrolytes for electrochemical cell applications. Curr Appl Phys 9:165–171. doi:10.1016/j.cap.2008.01.006

60. Kumar M, Tiwari T, Srivastava N (2012) Electrical transport behaviour of bio-polymer electrolyte system: Potato starch+ammonium iodide. Carbohydr Polym 88:54–60. doi:10.1016/j.carbpol.2011.11.059
61. Watanabe M, Nishimoto A (1995) Effects of network structures and incorporated salt species on electrochemical properties of polyether-based polymer electrolytes. Solid State Ionics 79:306–312. doi:10.1016/0167-2738(95)00089-L
62. Kufian MZ, Aziz MF, Shukur MF, Rahim AS, Ariffin NE, Shuhaimi NEA, Majid SR, Yahya R, Arof AK (2012) PMMA-LiBOB gel electrolyte for application in lithium ion batteries. Solid State Ionics 208:36–42. doi:10.1016/j.ssi.2011.11.032
63. Arof AK, Shuhaimi NEA, Alias NA, Kufian MZ, Majid SR (2010) Application of chitosan/iota-carrageenan polymer electrolytes in electrical double layer capacitor (EDLC). J Solid State Electrochem 14:2145–2152. doi:10.1007/s10008-010-1050-8